RAREFIED HYPERSONIC FLOW OVER CAVITIES

Rodrigo Cassineli Palharini

National Institute for Space Research (INPE/LCP)
Cachoeira Paulista - SP. Brasil
rodrigo@lcp.inpe.br

Wilson F. N. Santos

National Institute for Space Research (INPE/LCP)
Cachoeira Paulista - SP, Brasil
wilson@lcp.inpe.br

Abstract: *A computational study has been carried out to investigate a rarefied hypersonic flow over cavities by employing the Direct Simulation Monte Carlo (DSMC) method. The proposed work focuses on the effect in the flowfield structure due to variations in the cavity length-to-depth (L/H) ratio. The results presented highlight the sensitivity of the primary flow properties, velocity, density, pressure and temperature, to changes on the L/H ratio. It was found that the recirculation region inside the cavity is a function of the L/H ratio. The analysis showed that, for $L/H < 3$, the cavity flow structure represented that one observed in a "open" cavity. On the other hand, for $L/H = 4$, the cavity flow structure corresponded that of a "close" cavity for the conditions investigated.*

Keywords: *DSMC, Hypersonic flow.*

1 Introduction

In the design of a hypersonic vehicle, the knowledge of the factors that affect the thermal and aerodynamic loads acting on the vehicle surface becomes imperative. Usually, in the calculations of the thermal and aerodynamic loads, the analysis assumes that the vehicle has a smooth surface. However, imperfections, protuberances or discontinuities, such as cavities, gaps or steps, are often present on the vehicle surface due to, for instance, fabrication tolerances, sensor installations, and differential expansion or ablation rates between non-similar materials. Such surface discontinuities may constitute in a potential source in a heat flux rise to the surface or even though in a premature transition from laminar to turbulent flow.

Hypersonic flow over cavities, gaps or steps may cause locally thermal and aerodynamic loads which may dramatically exceed the ones of a smooth contour. In order to operate safely, these loads have to be predicted correctly. This can be done either by experiments which are often very expensive for real flight conditions or by numerical simulation, which is getting continuously increasing importance.

For the particular case of cavities, a large amount of experimental and numerical research studies is available in the published literature (Chapmann *et al.*, 1958; Charwat *et al.*, 1961a,b; Bertram and Wiggs, 1963; Hahn, 1969; Nestler *et al.*, 1969; Charwat, 1971; Nestler, 1982; Morgenstern Jr. and Chokani, 1994; Jackson *et al.*, 2001; Everhart *et al.*, 2006; Lee and Chandra, 2006; Cheng and Hung, 2006; Everhart, 2009; Plentovich *et al.*, 1993). These research studies have been conducted in order to understand the physical aspects of a subsonic, supersonic or hypersonic flow past to this type of surface discontinuity.

Based on a literature survey (Everhart *et al.*, 2006), length-to-depth (L/H) ratio is used to classify cavity flow physics. "Open" cavity flows occur in cavities with $1 < L/H < 10$ (typically) and are characterized by strong pressure and high levels of heat transfer at the trailing edge. The mainstream flow does not enter the cavity directly. "Close" cavity flows occur in cavities with $L/H > 14$ (typically) and are also regarded as stable flows. The pressure distribution along the floor of a "close" cavity shows a large longitudinal pressure gradient that causes a large increase in pressure drag and can lead to store separation difficulties. Also, the external flow is able to impinge on the cavity floor. Moreover, if cavity is long enough, a flow structure similar to that one observed for backward- and forward-facing steps may appear at the vicinity of the cavity sidewalls. Cavity geometries in the range $10 < L/H < 14$ are described as "transitional" and, for this particular case, the cavity flows exhibit a combination of "open" and "close" flow features. Usually, the precise boundaries between open, transitional, and closed flows depend on freestream Mach number and cavity width-to-depth (W/H) ratio (Plentovich *et al.*, 1993). Nevertheless, open flow always occurred for $L/H < 10$.

In order to understand the physical aspects of hypersonic flow past to cavities, the majority of the available research studies has gone into considering laminar or turbulent flow in the continuum flow

regime. However, there is little understanding of the physical aspects of hypersonic flow past to cavities related to the severe aerothermodynamic environment associated to a reentry vehicle. In this fashion, the purpose of the present account is to investigate the flowfield structure of a hypersonic flow on cavities in the transition flow regime, i.e., between the continuum flow and the free collision flow regime. Therefore, the focus of the present study is the low-density region in the upper atmosphere, where numerical gaskinetic procedures are available to simulate hypersonic flows. High-speed flows under low-density conditions deviate from a perfect gas behavior because of the excitation of rotational and vibrational modes. At high altitudes, and therefore, low density, the molecular collision rate is low and the energy exchange occurs under non-equilibrium conditions. In such a circumstance, the degree of molecular non-equilibrium is such that the Navier-Stokes equations are inappropriate. Consequently, the Direct Simulation Monte Carlo (DSMC) method will be employed to calculate the hypersonic two-dimensional flow on a cavity.

2 Geometry Definition

Discontinuities or imperfections present on the surface of a reentry capsule is modeled in the present account by a cavity defined by a length L and a depth H. By considering that the depth H is much smaller than the nose radius R of a reentry capsule, i.e., $H/R \ll 1$, then the hypersonic flow over the cavity may be considered as a hypersonic flow over a flat plate with a cavity. Figure 1 displays a schematic view of the model employed and presents the important geometric parameters.

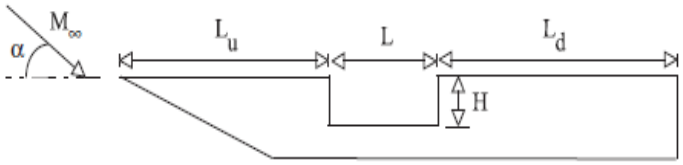

Figure 1: Drawing illustrating the cavity.

According to Fig. 1, M_∞ represents the freestream Mach number, H the cavity depth, L the cavity length, L_u the length of the cavity upstream surface, and L_d the length of the cavity downstream surface. It was considered that the flat plate is infinitely long but only the total length $L_u + L + L_d$ is examined. It was assumed a depth H of 3 mm, length L of 3, 6, 9, and 12 mm, L_u/λ_∞ of 50 and L_d/λ_∞ of 100, where λ_∞ is the freestream mean free path. Therefore, it was investigated cavities with L/H ratio of 1, 2, 3 and 4.

3 Computational Tool

Flows are characterized by a variety of dimensionless quantities. The most useful one for the purpose of this work is the Knudsen number Kn. The degree of rarefaction of a flow is usually expressed through the overall Knudsen number, $Kn = \lambda/l$, where λ is the mean free path in the freestream gas and l is a characteristic length of the flowfield. The conventional continuum flow assumption is valid when the overall Knudsen number tends to zero. In this flow regime, one can disregard its microscopic structure and consider only its macroscopic properties such as density, velocity, pressure, or temperature. In the opposite limit, the overall Knudsen number tending to infinity, the flow regime corresponds to the free molecular flow. In this case, intermolecular collisions may be neglected and particle collisions with the body surface play the determining role. The region defined by $0.1 < Kn < 10$ is referred to as the transition flow regime, where not only gas-surface collisions but also intermolecular collisions are important.

It is well known that neither the continuum flow equations nor the collisionless flow equations are valid to predict the flowfield characteristics throughout the transitional flow regime. During the last several years, the most successful numerical technique applied for computing flowfield structure in the transition flow regime has been the Direct Simulation Monte Carlo (DSMC) method pioneered by Bird in the 1960's (Bird, 1994). The DSMC method simulates real gas flows with various physical processes by means of a huge number of modeling particles, each of which is a typical representative of a great number of real gas molecules. DSMC models the flow as being a collection of discrete particles, each one with a position, velocity and internal energy. The state of particles is stored and modified with time as the particles move, collide, and undergo boundary interactions in simulated physical space.

In the present account, the molecular collision kinetics are modeled by using the variable hard sphere (VHS) molecular model (Bird, 1981), and the no time counter (NTC) collision sampling technique (Bird, 1989). Energy exchange between kinetic and internal modes is controlled by the Borgnakke-Larsen statistical model (Borgnakke and Larsen, 1975). Simulations are performed using a non-reacting gas model, consisting of 76.3% of N_2 and 23.7% of O_2, while considering energy exchange between translational, rotational and vibrational modes. For a given collision, the probability is defined by the inverse of the number of relaxation, which corresponds to the number of collisions needed, on average, for a molecule undergoes relaxation. The probability of an inelastic collision determines the rate at which energy is transferred between the translational and internal modes after an inelastic collision. Relaxation collision numbers of 5 and 50 were used for the calculations of rotation and vibration, respectively.

4 Computational Flow Domain and Grid

In order to implement the particle-particle collisions, the flowfield around the cavity is divided into an arbitrary number of regions, which are subdivided into computational cells. The cells are further subdivided into subcells, two subcells/cell in each coordinate direction. The cell provides a convenient reference for the sampling of the macroscopic gas properties, while the collision partners are selected from the same subcell for the establishment of the collision rate. The computational domain used for the calculation is made large enough so that body disturbances do not reach the upstream and side boundaries, where freestream conditions are specified. A schematic view of the computational domain is depicted in Fig. 2. According to this figure, the computational domain was divided into four regions. In addition, side I-A is defined by the cavity surface. Diffuse reflection with complete thermal accommodation is the condition applied to this side. Side I-B is a plane of symmetry, where all flow gradients normal to the plane are zero. At the molecular level, this plane is equivalent to a specular reflecting boundary. Sides II and III are the freestream side through which simulated molecules enter and exit. Finally, the flow at the downstream outflow boundary, side IV, is predominantly supersonic and vacuum condition is specified (Bird, 1994). At this boundary, simulated molecules can only exit.

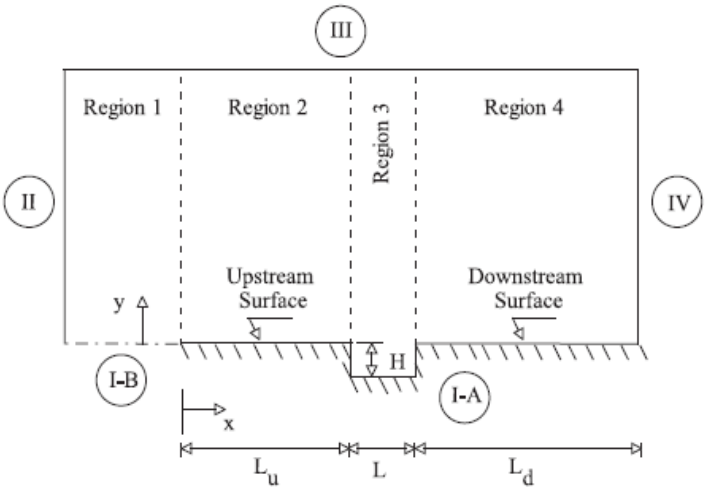

Figure 2: Drawing illustrating the computational domain.

DSMC results depends on the cell size chosen, on the time step as well as on the number of particles per computational cell. In the DSMC code, the linear dimensions of the cells should be small in comparison with the scale length of the macroscopic flow gradients normal to the streamwise directions, which means that the cell dimensions should be the order of or smaller than the local mean free path (Alexander *et al.*, 1998, 2000). The time step should be chosen to be sufficiently small in comparison with the local mean collision time (Garcia and Wagner, 2000; Hadjiconstantinou, 2000). A very small time step results in an inefficient advancement of the solution and accumulation of statistics. Most particles will take many time steps to cross a given cell. As a result, the collision phase of each time step will involve the same group of particles as in the previous time step since almost no particles leave or enter the cell. Moreover, a large time step allows the molecules to move too far without the opportunity to participate in a collision. This again causes a smearing of the properties of the flow, resulting in non-physical results; therefore, the time step must be chosen such that a typical particle moves about one fourth of the cell dimension

Table 1: Number of cells in the (x-direction) and [y-direction] for the $L/H = 1$ case.

	Region 1	**Region 2**	**Region 3**	**Region 4**
Coarse	(5×40)	(60×50)	(10×70)	(60×60)
	[10×20]	[120×25]	[20×35]	[120×30]
Standard	10×40	120×50	20×70	120×60
Fine	(20×40)	(240×50)	(40×70)	(240×60)
	[10×80]	[120×100]	[20×140]	[120×120]

at each time step. Finally, the number of simulated particles has to be large enough to make statistical correlations between particles insignificant.

A grid independence study was made with three different structured meshes – coarse, standard and fine – in each coordinate direction. The effect of altering the cell size in the x-direction was investigated for a coarse and fine grids with, respectively, 50% less and 50% more cells with respect to the standard grid only in the x-direction. Table 1 tabulates the number of cells employed in the four regions for coarse, standard, and fine grids for the $L/H = 1$ case.

In analogous fashion, an examination was made in the y-direction with a coarse and fine grids with, respectively, 50% less and 50% more cells with respect to the standard grid only in the y-direction. In addition, each grid was made up of non-uniform cell spacing in both directions. Moreover, point clustering is used close to solid walls and to the horizontal plane connecting the two corners. The effect (not shown) of changing the cell size in both directions on the heat transfer, pressure and the skin friction coefficients was rather insensitive to the range of cell spacing considered, indicating that the standard grid, with a total of 15,000 cells, for the $L/H = 1$ case, is essentially grid independent. In a second stage of the grid independence investigation, a similar examination was made for the number of molecules. The standard grid for the $L/H = 1$ case corresponds to, on average, a total of 314,700 molecules. Two new cases using the same grid were investigated. These two new cases correspond to 157,500 and 630,000 molecules in the entire computational domain. As the three cases presented approximately the same results (not shown) for the heat transfer, pressure and skin friction coefficients, hence the standard grid with a total of 314,700 molecules is considered enough for the computation of the flowfield properties.

5 Freestream and Flow conditions

The freestream conditions employed in the present calculations are those given by Leite and Santos (2009) and listed in Tab. 2, and the gas properties (Bird, 1994) considered in the simulation are shown in Tab. 3.

The freestream velocity U_∞ is assumed to be constant at 7456 m/s, which corresponds to a freestream Mach number M_∞ of 25. The wall temperature T_w is assumed constant at 880 K. This temperature is chosen to be representative of the surface temperature near the stagnation point of a reentry vehicle and is assumed to be uniform over the cavity surface. It is important to mention that the surface temperature is

Table 2: Freestream flow conditions

Altitude (km)	T_∞(K)	p_∞(N/m^2)	ρ_∞(kg/m^3)	μ_∞(Ns/m^2)	n_∞(m^{-3})	λ_∞(m)
70	219.07	5.518	8.752×10^{-5}	1.628×10^{-5}	1.8193×10^{21}	9.285×10^{-4}

Table 3: Gas properties

	X	m (kg)	d (m)	ω
O_2	0.237	5.312×10^{-26}	4.01×10^{-10}	0.77
N_2	0.763	4.650×10^{-26}	4.11×10^{-10}	0.74

low compared to the stagnation temperature of the air. This assumption seems reasonable since practical surface material will probably be destroyed if surface temperature is allowed to approach the stagnation temperature.

By assuming the cavity length L as the characteristic length, the Knudsen number Kn_L corresponds to 0.3095, 0.1548, 0.1032, and 0.0774 for length L of 3, 6, 9, and 12 mm, respectively. Finally, the Reynolds number Re_L is around 121.7, 243.4, 365.1, and 486.8 for length L of 3, 6, 9, and 12 mm, respectively, also based on conditions in the undisturbed stream.

6 Computational Results and Discussion

The purpose of this section is to discuss and to compare differences in the primary properties due to changes on the L/H ratio of the cavity. The primary properties of particular interest in this work are velocity, density, pressure, and temperature.

6.1 Velocity Field

The DSMC method is essentially a statistical method. In this way, the macroscopic properties are computed as averages from the microscopic properties in each cell in the computational domain. As a result, the velocity vector is given by the following expression,

$$\mathbf{c}_0 = \frac{\sum_{j=1}^{N} (m\mathbf{c})_j}{\sum_{j=1}^{N} m_j} \tag{1}$$

where N, m and $\mathbf{c}$ represent, respectively, the number of molecules, the mass and the velocity vector of the molecules in each cell. It should be noted that the mean molecular velocity $\mathbf{c}_0$ $(= u\vec{i} + v\vec{j} + w\vec{k})$ defines the macroscopic mean velocity.

The distribution of tangential velocity u/U_∞ for two sections inside the cavity is illustrated in Fig. 3 as a function of the L/H ratio. In this set of plots, X'_L represents the distance $(x - L_u - L/2)$ normalized by the cavity length L, and Y'_H the distance $y + H$ above the cavity surface normalized by depth H. In this context, the reference frame was moved to the center of the cavities. It is important to mention that section X'_L = -0.4 is immediately behind the back face of the cavities and section $X'_L = 0.4$ is located immediately ahead of the frontal face of the cavities. According to Fig. 3, for $Y'_H \simeq 0$, the tangential velocity ratio is negative. Approaching the top of the cavities, the velocity ratio u/U_∞ becomes positive at a section Y'_H that depends on the L/H ratio. Still further upward, the tangential velocity u increases significantly and tends to the freestream velocity U_∞ close to the upper boundary of the computational domain. As a base of comparison, for the velocity profiles at X'_L = -0.4, the velocity ratio u/U_∞ changes from negative to positive values at section Y'_H of 0.82, 0.72, 0.64, and 0.53 for L/H ratio of 1, 2, 3, and 4, respectively. On the other hand, for the velocity profiles at $X'_L = 0.4$, Y'_H changes to 0.70, 0.53, 0.42, and 0.32 for L/H ratio of 1, 2, 3, and 4, respectively. Therefore, it is firmly established that the thickness of the separated boundary layer grows with the L/H ratio rise and with the profile position inside the cavities.

In order to emphasize important features in the flowfield structure, streamline traces at the vicinity of the cavities are demonstrated in Fig. 4. In this group of diagrams, Y_H stands for the vertical distance y normalized by the cavity depth H, and X'_H is the length $(x - L_u)$ normalized by the cavity depth H. According to Fig. 4, it is clearly noticed that the flow inside cavities is characterized by the appearance of recirculation regions. The streamline pattern for the $L/H = 1$ case, Fig. 4(a), shows that the flow is characterized by a primary vortex system. A similar flow structure is noticed for the $L/H = 2$ case, as displayed by Fig. 4(b). Nevertheless, in contrast to the previous case, the vortex core approached the frontal face of the cavity, i.e., the downstream face. For the $L/H = 1$ and 2 cases, it is noteworthy that the recirculating structure fills the entire cavities. In the following, for the $L/H = 3$ case, Fig. 4(c), a different flow structure is observed; two vortices are formed, one of them closed to the frontal face and the other one at the vicinity of the back face of the cavity, i.e., the upstream face. The external stream does not reattach and the flow is reversed along all the floor of the cavity. It should be remarked that "upstream" and "downstream" always refer to the sense of the freestream direction. Finally, for the $L/H = 4$ case, Fig. 4(d), the recirculation regions are well defined when compared to the previous case. In addition, for this particular case, the external stream reattaches the cavity floor. It should be remarked that the flow characteristics observed for the $L/H = 4$ case represent those for a "close" cavity. Nevertheless, in the continuum flow regime, "close" cavity flows occur in cavities with $L/H > 14$ (Everhart *et al.*, 2006).

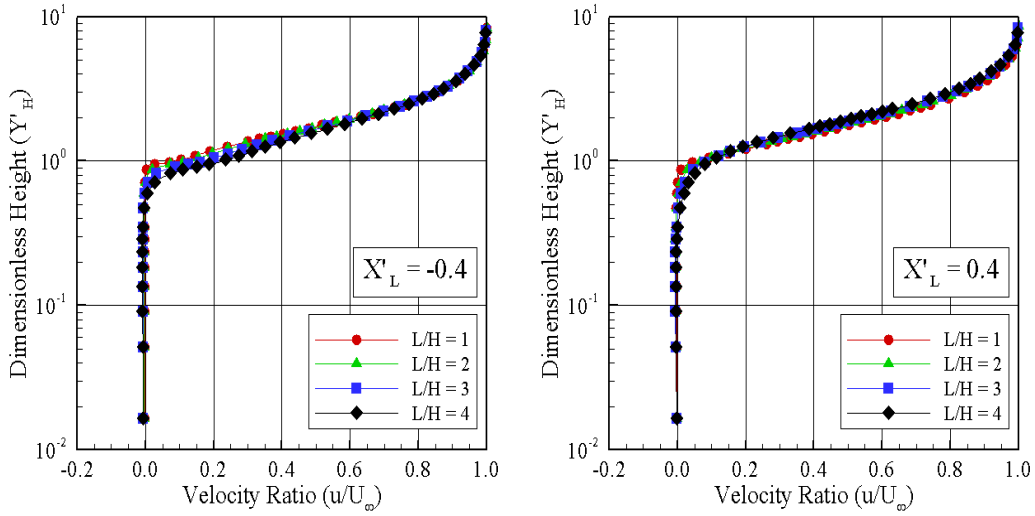

Figure 3: Tangential velocity (u/U_∞) profiles for section X'_L of (a) -0.4 and (b) 0.4 inside the cavities.

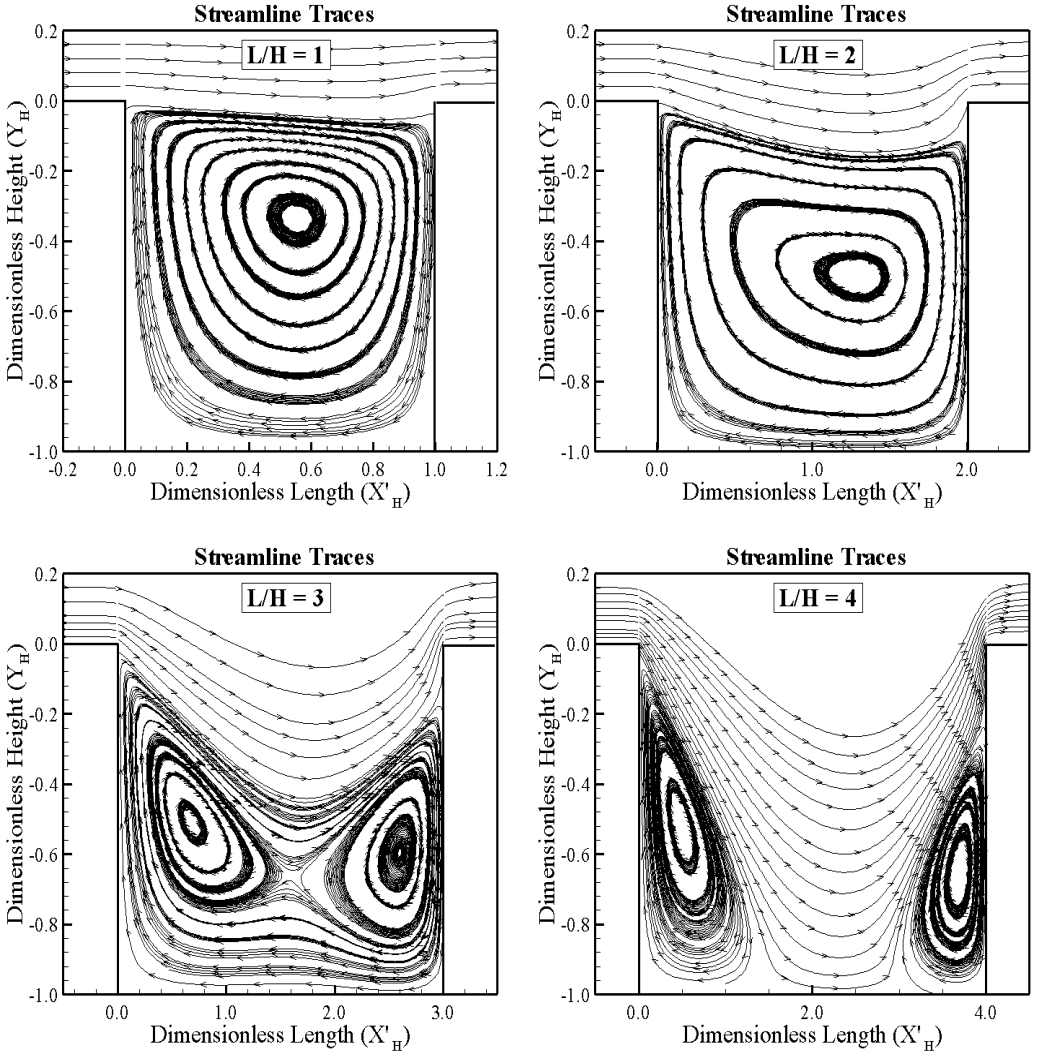

Figure 4: Distribution of streamline traces at the vicinity of the cavities for L/H ratio of (a) 1, (b) 2, (c) 3, and (d) 4.

6.2 Density Field

The density in each cell in the computational domain is obtained by the following expression,

$$\rho = \frac{1}{V_c} \sum_{j=1}^{N} m_j \tag{2}$$

where N is the number of molecules in the cell, m is the mass of the molecules and V_c is the volume of the cell.

The impact on density profiles ρ/ρ_∞ due to changes in the L/H ratio is displayed in Fig. 5. Similar to the distribution of tangential velocity, the distribution of density profiles is shown in this set of plots for two sections defined by X'_L = -0.4 and 0.4. Based on these plots, it is apparent that density ratio shows significant changes not only in the direction perpendicular to the cavity surface but also along the surface inside the cavity. For the section X'_L = -0.4, it is seen that the density ratio decreases with the L/H ratio rise. Particular attention is paid to the L/H of 3 and 4. For these cases, density ρ is smaller than the freestream density ρ_∞. This is explained by the fact that with increasing the L/H ratio, the flow penetrates more deeply inside the cavity due to the flow expansion around the corner of the back face of the cavity. As a result, a recirculation zone is formed characterized by a zone of low density. Conversely, for the section X'_L = 0.4, the flow experiences a compression, and the density ρ increases well above the freestream density ρ_∞ with increasing the L/H ratio.

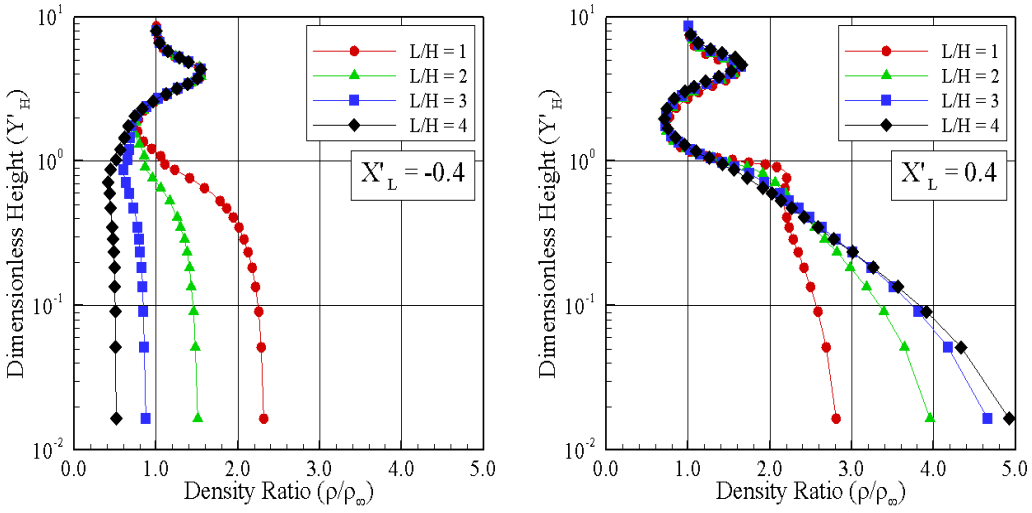

Figure 5: Density ratio (ρ/ρ_∞) profiles for section X'_L of (a) -0.4 and (b) 0.4 inside the cavities.

6.3 Pressure Field

The pressure in each cell inside de computational domain is obtained by the following equation,

$$p = \frac{1}{3V_c} \sum_{j=1}^{N} \frac{(mc^2)_j}{N} \tag{3}$$

where N is the number of molecules in the cell, m is the mass of the molecules and V_c is the volume of the cell and c is the velocity of the molecules.

The influence of the L/H ratio on pressure ratio p/p_∞ profiles is depicted in Fig. 6 for two sections defined by X'_L = -0.4 and 0.4. It is apparent from this group of diagrams that pressure profiles follow the same trend as those presented by density in the sense that, pressure significantly decreases close to the cavity back face due to the flow expansion, and that pressure dramatically increases at the vicinity of the cavity frontal face as a result of the flow compression.

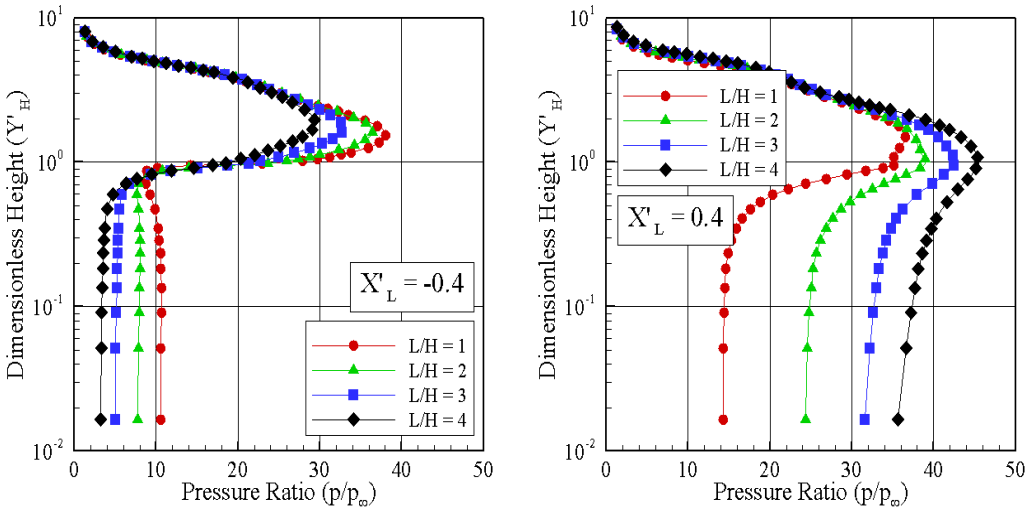

Figure 6: Pressure ratio (p/p_∞) profiles for section X' of (a) -0.4 and (b) 0.4 inside the cavities.

6.4 Kinetic Temperature Field

Temperature ratio profiles inside the cavities are displayed in Fig. 7 for two sections defined by X'_L = -0.4 and 0.4. In this group of plots, temperature ratio stands for the translational temperature T_T, rotational temperature T_R, vibrational temperature T_V or overall temperature T_O normalized by the freestream temperature T_∞. Also, filled and empty symbols correspond to temperature distributions for L/H ratio of 1 and 4, respectively. It is apparent from these plots that thermodynamic non-equilibrium occurs inside the cavities, as shown by the lack of equilibrium of the translational and internal kinetic temperatures. Thermal non-equilibrium occurs when the temperatures associated with translational, rotational, and vibrational modes of a polyatomic gas are different. In such a context, it proves convenient to define the overall kinetic temperature. The overall kinetic temperature shown is defined (Bird (1994)) for a non-equilibrium gas as the weighted mean of the translational and internal temperature as follows,

$$T_O = \frac{3T_T + \zeta_R T_R + \zeta_V T_V}{3 + \zeta_R + \zeta_V} \tag{4}$$

were ζ is the degree of freedom and subscript T, R and V stand for translation, rotation and vibration, respectively.

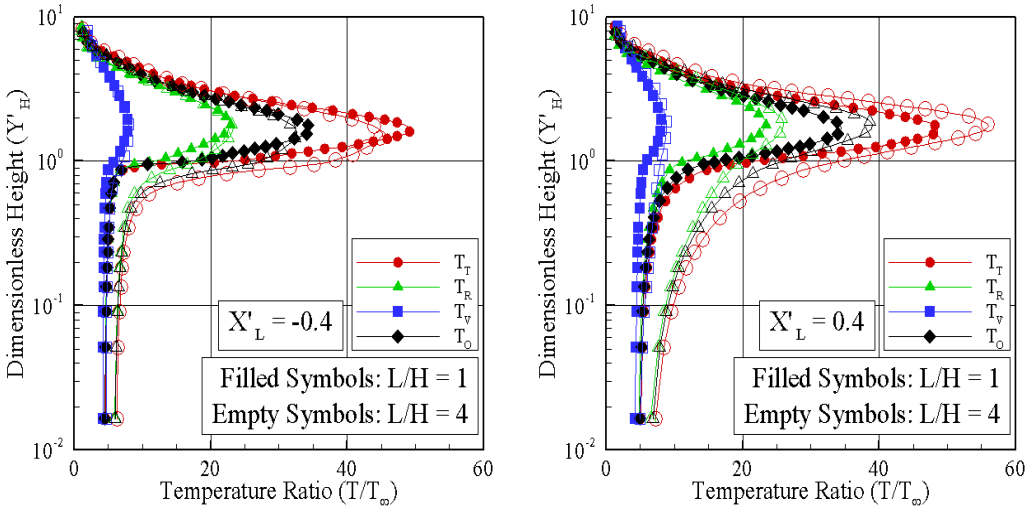

Figure 7: Kinetic temperature ratio (T/T_∞) profiles for section X'_L of (a) -0.4 and (b) 0.4 inside the cavities.

The overall kinetic temperature T_O is equivalent to the thermodynamic temperature only in thermal equilibrium conditions. As a matter of fact, it should be noticed that the ideal gas equation of state does not apply to this temperature in anon-equilibrium situation.

7 Concluding Remarks

A detailed numerical study has been carried out to investigate a rarefied hypersonic flow over cavities by using the Direct Simulation Monte Carlo (DSMC) method. The simulations provided information concerning the nature of the primary properties inside the cavities. Effects of the length-to-depth (L/H) ratio on velocity, density, pressure and temperature were investigated for a representative range of parameters. The L/H ratio ranged from 1 to 4, which corresponded to Knudsen numbers in the transition flow regime.

The analysis showed that the recirculation region inside the cavities is a function of the L/H ratio. It was found that, for $L/H < 3$, the cavity flow structure represented that one observed in a "open" cavity. Conversely, for $L/H = 4$, the cavity flow structure corresponded to that of a "close" cavity. The results showed that cavity flow behavior in the transition flow regime differed from that found in the continuum flow regime. Future work is being undertaking to study the aerodynamic surface quantities on the cavities.

Acknowledgment

The authors would like to thank the financial support provided by FAPESP (Fundação de Amparo a Pesquisa do Estado de São Paulo) under Grant No. 2007/57673-6.

References

Alexander, F. J., Garcia, A. L., and Alder, B. J., 1998,"Cell Size Dependence of Transport Coefficient in Stochastic Particle Algorithms", Physics of Fluids, vol. 10, no. 6, pp. 1540–1542.

Alexander, F. J., Garcia, A. L., and Alder, B. J., 2000,"Erratum: Cell Size Dependence of Transport Coefficient in Stochastic Particle Algorithms", Physics of Fluids, vol. 12, no. 3, pp. 731–731.

Bertram, M. H. and Wiggs, M. M., 1963, "Effect of Surface Distortions on the Heat Transfer to a Wing at Hypersonic Speeds", AIAA Journal, vol. 1, no. 6, pp. 1313–1319.

Bird, G. A., 1981,"Monte Carlo Simulation in an Engineering Context", Fisher, S. S., ed., Progress in Astronautics and Aeronautics: Rarefied gas Dynamics, vol. 74, part I, AIAA New York, pp. 239–255.

Bird, G. A., 1989,"Perception of Numerical Method in Rarefied Gasdynamics", Muntz, E. P., Weaver, D. P. & Capbell, D. H., eds., Rarefied Gas Dynamics: Theoretical and Computational Techniques, vol. 118, Progress in Astronautics and Aeronautics, AIAA, New York, pp. 374–395.

Bird, G. A., 1994, Molecular Gas Dynamics and the Direct Simulation of Gas Flows, Oxford University Press.

Borgnakke, C. and Larsen, P. S., 1975,"Statistical Collision Model for Monte Carlo Simulation of Polyatomic Gas Mixture",Journal of Computational Physics, vol. 18, no. 4, pp. 405–420.

Chapmann, D. R., Kuehn, D. M. and Larson, H. K., 1958, "Investigation of Separeted Flows in Supersonic and Subsonic Streams with Emphasis on the Effect of Transition", NACA Report 1356.

Charwat, A. F., Dewey, C. F., Roos, J. N. and Hitz, J. A., 1961, "An Investigation of Separated Flows – Part I: The Pressure Field", Journal of aerospace Sciences, vol. 28, no. 6, pp. 457–470.

Charwat, A. F., Dewey, C. F., Roos, J. N. and Hitz, J. A., 1961, "An Investigation of Separated Flows – Part II: Flow in the Cavity and Heat Transfer", Journal of aerospace Sciences, vol. 28, no. 7, pp. 513–527.

Charwat, A. F., 1961, "Separation of a Supersonic Accelerated Flow over Notches", AIAA Journal, vol. 9, no. 8, pp. 1656–1657.

Cheng, M., and Hung, K. C., 2006,"Vortex Structure of Steady Flow in a Rectangular Cavity", Computers and Fluids, vol. 35, no. , pp. 1046–1062.

Everhart, J. L., Alter, S. J., Merski, N. R., and Wood, W. A.,"Pressure Gradient Effects on Hypersonic Flow Heating", 44th AIAA Aerospace Sciences Meeting and Exhibit, AIAA Paper 2006–0185.

Everhart, J. L., 2009,"Supersonic/Hypersonic Laminar heating Correlations for Rectangular and Impact-Induced Open and Closed Cavities", Journal of spacecraft and Rockets, vol. 46, no. 3, pp. 545–560.

Garcia, A. L. and Wagner, W., 2000,"Time Step Truncation Error in Direct Simulation Monte Carlo", Physics of Fluids, vol. 12, no. 10, pp. 2621–2633.

Hadjiconstantinou, N. G., 2000,"Analysis of Discretization in the Direct Simulation Monte Carlo", Physics of Fluids, vol. 12, no. 10, pp. 2634–2638.

Hahn, M., 1969,"Experimental Investigation of Separated Flow over a Cavity at Hypersonic Speed", AIAA Journal, vol. 7, no. 6, pp. 1092–1098.

Jackson, A. P., Hillier, R., and Soltani, S., 2001,"Experimental and Computational Study of Laminar Cavity Flows at Hypersonic Speeds", Journal Fluid Mechanics, vol. 427, no. , pp. 329–358.

Leite, P. H. M., and Santos, W. F. N., 2009,"Direct Simulation Calculations of the Rarefied Hypersonic Flow past a Backward-Facing Step", Brazilian Symposium on Aerospace Engineering and Applications, September 14–16, São José dos Campos, SP, Brazil.

Lee, G., and Chandra, S., 2006,"Numerical Analysis of Heat Transfer Enhancement from Surfaces with Cavities", 44th AIAA Aerospace Sciences Meeting and Exhibit, AIAA Paper 2006–0186.

Morgenstern Jr., A. and Chokani, N., 1994,"Hypersonic Flow Past Open Cavities", AIAA Journal, vol. 32, no. 12, pp. 2387–2393.

Nestler, D. E., Saydah, A. R., and Auxer, W. L., 1969,"Heat Transfer to Steps and Cavities in Hypersonic Turbulent Flow", AIAA Journal, vol. 7, no. 7, pp. 1368–1370, 1969.

Nestler, D. E., 1982,"An Experimental Study of Hypersonic Cavity Flow", Journal of Spacecraft and Rockets, vol. 19, no. 3, pp. 195–196.

Plentovich, E. B., Stallings, R. L. and Tracy, M. B., 1993,"Experimental cavity pressure measurements at subsonic and transonic speeds", NASA Technical Report, No. TP-3358.